

DDFT calibration and investigation of an anisotropic phase-field crystal model

Muhammad Ajmal Choudhary¹, Daming Li¹, Heike Emmerich¹
and Hartmut Löwen²

¹ Lehrstuhl für Material- und Prozesssimulation, Universität Bayreuth, D-95440
Bayreuth, Germany

² Institut für Theoretische Physik II: Weiche Materie, Heinrich-Heine-Universität
Düsseldorf, D-40225 Düsseldorf, Germany

E-mail: ajmal.choudhary@uni-bayreuth.de

Abstract.

The anisotropic phase-field crystal model recently proposed and used by Prieler et al. [J. Phys.: Condens. Matter **21**, 464110 (2009)] is derived from microscopic density functional theory for anisotropic particles with fixed orientation. Further its morphology diagram is explored. In particular we investigated the influence of anisotropy and undercooling on the process of nucleation and microstructure formation from atomic to the microscale. To that end numerical simulations were performed varying those dimensionless parameters which represent anisotropy and undercooling in our anisotropic phase-field crystal (APFC) model. The results from these numerical simulations are summarized in terms of a morphology diagram of the stable state phase. These stable phases are also investigated with respect to their kinetics and characteristic morphological features.

PACS numbers: 81.10.Aj, 64.70.dm, 82.70.Dd

1. INTRODUCTION

Early in the 90th Swift and Hohenberg formulated an amplitude approach to describe systems, where the stable states are periodic, as e.g. the case for Rayleigh-Bénard convection [1]. More recently this idea has been taken up by the materials science community to model crystals at the atomic scale. Elder et al. proposed a functional for a scalar dimensionless field ϕ of form

$$F = \int_V \left(\frac{1}{2} \phi [(q_0^2 + \nabla^2)^2 - \varepsilon] \phi + \frac{1}{4} \phi^4 \right) dr, \quad (1)$$

with two phenomenological parameters q_0 and ε and a corresponding dynamical equation

$$\frac{\partial \phi}{\partial t} = \nabla^2 \frac{\delta F}{\delta \phi} \quad (2)$$

for this purpose [2]. Since its introduction, this phase-field crystal (PFC) method [2, 3, 4, 5, 6] has emerged as a computationally efficient alternative to molecular dynamics (MD) simulations for problems where the atomic and the continuum scale are tightly coupled. The reason is that it operates for atomic length scales and diffusive time scales. Thus for a simple application such as diffusion in gold or copper it runs 10^6 - 10^8 times faster than the corresponding MD calculation [7]. In that sense it provides from point of view of multiscale materials modeling an interesting link between the traditional phase-field method and MD. Moreover, a connection between classical density functional theory of freezing and phase-field crystal modeling could be identified in [4, 8]. Thereby a second theoretical foundation besides the Swift-Hohenberg amplitude equation approach could be established. Essentially it motivates the application of PFC models also for spatially non-uniform *non-periodic* states.

Recently the phase-field crystal method has been applied to a variety of different growth phenomena. One of its interesting features is that other than the phase-field method, in which elasticity explicitly needs to be integrated in the functional to be taken into account [9], it includes elastic effects inherently. Thus it allows to simulate for example features of crack propagation [4] and plasticity [3, 10] from the atomic to the micro-scale. To model the elastic behavior of different kinds of materials, the parameters of the phase-field crystal model equation can be adjusted to match the elastic moduli of a given experimental system. However, in its most simplistic form, in which it is a reformulation of the Swift-Hohenberg equation [1] with a conserved dynamics as introduced by Elder *et al.* [2, 3] the Poisson ratios which can be modeled, are restricted to $1/3$ (in the one mode approximation). Moreover, since in the simplistic PFC model the material is defined by only three parameters, it is restricted with respect to the crystal lattice structures which it can describe as well. These are triangular symmetries in two dimensions and *BCC* symmetry in three dimensions [11, 12]. Another crystal symmetry applying to protein crystals in a membrane could be obtained by including higher order correlation functions [13]. Moreover, liquid crystals have been simulated by combining the original phase-field crystal equation with an orientational field [14, 16, 15].

In [17] we followed the above direction to extend the phase-field to apply to a larger class of condensed matter systems taking a different route: We derived a generalized PFC model for isotropic as well as anisotropic crystal lattice systems of arbitrary Poisson ratios as well as condensed matter systems built-up from non-spherical units such as for example anisotropic colloids and liquid crystals. To this end we extended the simplest PFC model proposed by Elder [2], to a conservative, anisotropic Langevin equation and applied it to the heterogeneous nucleation of colloids at a wall.

Whereas our previous work [17] was devoted to a mere introduction of our model and its application to heterogenous nucleation at a wall, here we show for the first time how its parameters can be derived from dynamical density functional theory (DDFT) (see section 2). Further we report for the first time in detail on its morphology diagram. To do so, we proceed as follows: First we give a thorough derivation of our anisotropic phase-field model based on the DDFT in section 2. We then - after a brief summary of the model in section 2 - study the influence of anisotropy and undercooling on the morphology of the final states. We analyze these morphologies and summarize our results in terms of a morphology diagram in section 4. Finally we conclude with a summary and an outlook of our study in section 5.

2. ANISOTROPIC PHASE-FIELD CRYSTAL MODEL

2.1. The model

By now phase-field crystal (PFC) modeling is widely used to predict crystal nucleation growth and to model microstructural pattern formation during different physical phenomena such as solidification. As usual, the PFC model used in this studies is based on a free energy functional $F[\phi(r, t)]$ of phase-field $\phi(r, t)$ and a dynamical equation which represents the time evolution of the phase-field. In this PFC model, periodic nature of a crystal lattice is incorporated by using a free energy functional which is minimized by periodic density field. The equation of motion used in this model was introduced in [2] for the case of simplest phase-field crystal (SPFC) model, and is given by

$$\rho \frac{\partial \phi}{\partial t} = \Delta \left[\{ (q_0^2 + \Delta)^2 - \epsilon \} \phi + \phi^3 \right], \quad (3)$$

here, q_0 and ϵ are constants. In order to simplify the model, a dimensionless parameter τ is introduced which is defined as

$$\tau = - (q_0^2 - \epsilon). \quad (4)$$

In our model τ represents undercooling in the same manner as r is defined in [18], therefore, τ can be written as

$$\tau \propto \Delta T. \quad (5)$$

The anisotropic version of phase-field crystal model originally introduced in [19] is used in this study. This PFC model is basically an extension of the SPFC model which is derived in [20]. The APFC model is capable of simulating isotropic and anisotropic

crystal lattice system of any arbitrary poisson ratio as well as condensed matter systems such as colloids and liquid crystals. The free energy functional used in this model is given by

$$F = \int_V \left(\frac{1}{2} \phi \left[-\tau + a_{ij} \frac{\partial^2}{\partial x_i \partial x_j} + b_{ijkl} \frac{\partial^4}{\partial x_i \partial x_j \partial x_k \partial x_l} \right] \phi + \frac{1}{4} c \phi^4 \right) dr, \quad (6)$$

where a_{ij} is a symmetric matrix and b_{ijkl} is a fourth rank tensor with the symmetry of an elastic tensor: $i \leftrightarrow j, k \leftrightarrow l, (i, j) \leftrightarrow (k, l)$. From the free energy functional defined in Equation (6), the corresponding Langevin differential equation of motion for anisotropic lattice system can be written as follows:

$$\rho \frac{\partial \phi}{\partial t} = \Delta \left(\left[-\tau + a_{ij} \frac{\partial^2}{\partial x_i \partial x_j} + b_{ijkl} \frac{\partial^4}{\partial x_i \partial x_j \partial x_k \partial x_l} \right] \phi + c \phi^3 \right). \quad (7)$$

2.2. Derivation of the anisotropic phase-field crystal model from dynamical density functional theory

The coefficients occuring in the anisotropic phase-field crystal model proposed in Ref. [17] can be derived from microscopic density functional theory [21, 22, 23, 24]. Here we follow a similar line as proposed recently by van Teeffelen et al [8] for radially symmetric interactions. We generalize this route here to anisotropic interactions.

We assume that the anisotropic colloids are completely aligned in space. Cartesian coordinates $\mathbf{r} = (x_1, x_2, \dots, x_d)$ will be used in the following, d denoting the spatial dimension. The interaction pair potential between two aligned particles is $u(\mathbf{r})$ [25]. The latter function is anisotropic, in general, i.e. it does not only depend on $|\mathbf{r}|$. Other examples for these anisotropic interactions with fixed orientations are oriented hard spherocylinders [26] and charged rods [27, 28], anisotropic Gaussian potentials [29], board-like colloidal particles [30], colloidal molecules [31], as well as patchy colloids [32] and proteins [33, 34]. Henceforth *inversion* symmetry is assumed

$$u(-\mathbf{r}) = u(\mathbf{r}) \quad (8)$$

Dynamical density functional theory for anisotropic situations [35] is now generalized from the isotropic case as follows. The dynamical evolution of the time-dependent one-particle density field $\rho(\mathbf{r}, t)$ is:

$$\dot{\rho}(\mathbf{r}, t) = (k_B T)^{-1} \nabla \cdot \left[\mathcal{D} \rho(\mathbf{r}, t) \nabla \frac{\delta F[\rho(\mathbf{r}, t)]}{\delta \rho(\mathbf{r}, t)} \right]. \quad (9)$$

Here $k_B T$ is the thermal energy, and $\nabla = (\partial/\partial x_1, \partial/\partial x_2, \dots, \partial/\partial x_d)$ is the d -dimensional gradient. $\mathcal{D} = \text{diag}(D_1, D_2, \dots, D_d)$ denotes the diagonalized diffusion tensor with the anisotropic short-time translational diffusivities of the anisotropic particle. For a given (hydrodynamic) shape of the particle, explicit expressions for D_i are available [36, 37]. Furthermore, in Equation (9), $F[\rho(\mathbf{r}, t)]$ is the equilibrium density functional which can be split as

$$F[\rho(\mathbf{r})] = F_{\text{id}}[\rho(\mathbf{r})] + F_{\text{ex}}[\rho(\mathbf{r})] + F_{\text{ext}}[\rho(\mathbf{r})]. \quad (10)$$

where

$$F_{\text{id}}[\rho(\mathbf{r})] = k_B T \int d\mathbf{r} \rho(\mathbf{r}) \{ \ln [\rho(\mathbf{r}) \Lambda^d] - 1 \} , \quad (11)$$

with Λ denoting the thermal de Broglie wavelength. The external part involves an external one-body potential $V(\mathbf{r}, t)$ and is given by

$$F_{\text{ext}}[\rho(\mathbf{r})] = \int d\mathbf{r} \rho(\mathbf{r}) V(\mathbf{r}, t) . \quad (12)$$

Finally, the excess part $F_{\text{ex}}[\rho(\mathbf{r})]$, embodies the nontrivial correlations between the particles and must be further approximated. Henceforth we assume small deviations of the inhomogeneous density profile around a homogeneous reference density ρ . In this limit, the leading approximation for $F_{\text{ex}}[\rho(\mathbf{r})]$ is given by the Ramakrishnan and Yussouff [38] expression:

$$F_{\text{ex}}[\rho(\mathbf{r})] \simeq F_{\text{ex}}(\rho) - \frac{k_B T}{2} \int \int d\mathbf{r} d\mathbf{r}' \Delta\rho(\mathbf{r}) \Delta\rho(\mathbf{r}') c_0^{(2)}(\mathbf{r} - \mathbf{r}'; \rho) . \quad (13)$$

where $c_0^{(2)}(\mathbf{r} - \mathbf{r}'; \rho)$ is the anisotropic direct correlation function of the fluid at density ρ which possesses the same symmetry as the underlying pair potential $u(\mathbf{r})$. In particular, it is inversion-symmetric

$$c_0^{(2)}(-\mathbf{r}, \rho) = -c_0^{(2)}(\mathbf{r}, \rho) \quad (14)$$

Moreover, $\Delta\rho(\mathbf{r}) = \rho(\mathbf{r}) - \rho$. In Fourier space Equation (13) reads

$$\mathcal{F}_{\text{ex}}[\rho(\mathbf{r})] = F_{\text{ex}}(\rho) - \frac{k_B T (2\pi)^d}{2} \int d\mathbf{k} \Delta\tilde{\rho}(\mathbf{k}) \Delta\tilde{\rho}(-\mathbf{k}) \tilde{c}_0^{(2)}(\mathbf{k}, \rho) \quad (15)$$

with \sim denoting a Fourier transform. We now expand the direct correlation function $c_0^{(2)}(\mathbf{k}, \rho)$ in terms of \mathbf{k} around $\mathbf{k} = 0$. (Alternatively fitting procedures can be used, e.g. around the first peak of $c_0^{(2)}(\mathbf{k}, \rho)$.) This leads to the Taylor expansion in Fourier space

$$\tilde{c}_0^{(2)}(\mathbf{k}, \rho) = \hat{C}_0 + \sum_{i,j=1}^d a_{ij} k_i k_j + \sum_{i,j,k,l=1}^d b_{ijkl} k_i k_j k_k k_l + \dots \quad (16)$$

corresponding to a gradient expansion in real-space. Inversion symmetry Equation (14) enforces all odd orders to vanish. Possible additional symmetries in the shape of the particles will lead to corresponding restrictions on the tensorial coefficients a_{ij} and b_{ijkl} as discussed below.

Inserting this expansion into Equation (9), one gets

$$\begin{aligned} \dot{\rho}(\mathbf{r}, t) = & \nabla \cdot \mathcal{D} \nabla \rho(\mathbf{r}, t) + \nabla \cdot \mathcal{D} \nabla \left[(k_B T)^{-1} V(\mathbf{r}, t) \right. \\ & \left. - (\hat{C}_0 - \sum_{i,j=1}^d a_{ij} \frac{\partial^2}{\partial x_i \partial x_j} + \sum_{i,j,k,l=1}^d b_{ijkl} \frac{\partial^4}{\partial x_i \partial x_j \partial x_k \partial x_l}) \rho(\mathbf{r}, t) \right] . \end{aligned} \quad (17)$$

If one further uses the constant mobility approximation, $\rho(\mathbf{r}, t) = \rho$ in front of the functional derivative in Equation (9) and if one approximates

$$F_{\text{id}}[\rho(\mathbf{r})] \approx k_B T \rho \int d\mathbf{r} \left\{ \frac{1}{2} \phi(\mathbf{r}, t)^2 - \frac{1}{6} \phi(\mathbf{r}, t)^3 + \frac{1}{12} \phi(\mathbf{r}, t)^4 - \text{const.} \right\} \quad (18)$$

with $\phi(\mathbf{r}, t) = \Delta\rho(\mathbf{r}, t)/\rho$, one arrives at:

$$\begin{aligned} \dot{\phi}(\mathbf{r}, t) = & \rho \nabla \cdot \mathcal{D} \nabla \left[\phi(\mathbf{r}, t) - \frac{1}{2} \phi(\mathbf{r}, t)^2 + \frac{1}{3} \phi(\mathbf{r}, t)^3 + (k_B T)^{-1} V(\mathbf{r}, t) \right. \\ & \left. - \rho(\hat{C}_0 - \sum_{i,j=1}^d a_{ij} \frac{\partial^2}{\partial x_i \partial x_j} + \sum_{i,j,k,l=1}^d b_{ijkl} \frac{\partial^4}{\partial x_i \partial x_j \partial x_k \partial x_l}) \phi(\mathbf{r}, t) \right]. \end{aligned} \quad (19)$$

This exactly reduces to the anisotropic phase-field model of Ref. [17] for the special case $d = 2$, $\mathcal{D} = D_0 \infty$, and a neglected cubic term in the ideal gas functional expansion in Equation (18). As a remark the latter was retained in other variants of the PFC model [39, 40].

Concluding this section, the anisotropic phase-field crystal model as used in [17] can be derived and justified from dynamical density functional theory. The derivation points, however, to more realistic approximations for anisotropic diffusivities. Furthermore, if Equation (18) is used, some approximations can be avoided but these were not found to change the results significantly for spherical interactions [8].

2.3. Phenomenological symmetry considerations

We finally present phenomenological symmetry arguments for the expansion coefficients a_{ij} and b_{ijkl} of the anisotropic PFC model. First we assume that the orientation of the fixed particles is set by a single unit vector \vec{E} only which is invariant under space inversion ($\vec{r} \rightarrow -\vec{r}$). This is the case for $d = 2$ and for rotationally symmetric particles in $d = 3$. Then, any gradient term in the scalar free energy functional must involve an even number of gradients due to space inversion symmetry. Rotational symmetry of space then requires that only combinations of $\vec{E} \cdot \vec{\nabla}$ and $\vec{\nabla} \cdot \vec{\nabla}$ are nonvanishing in the functional. Therefore the only possibility for physically relevant gradient terms is

$$\sum_{i,j=1}^d a_{ij} \frac{\partial^2}{\partial x_i \partial x_j} = \lambda_1 (\vec{E} \cdot \vec{\nabla})^2 + \lambda_2 \Delta \quad (20)$$

and

$$\sum_{i,j,k,l=1}^d b_{ijkl} \frac{\partial^4}{\partial x_i \partial x_j \partial x_k \partial x_l} = \lambda_3 (\vec{E} \cdot \vec{\nabla})^4 + \lambda_4 (\vec{E} \cdot \vec{\nabla})^2 \Delta + \lambda_5 \Delta^2 \quad (21)$$

where λ_1 , λ_2 , λ_3 , λ_4 , and λ_5 are scalar prefactors. This reduces the number of independent degrees of freedom in a_{ij} and b_{ijkl} down to 5.

In case there are different fixed vectors, say \vec{E} and \vec{B} , there are correspondingly more terms allowing for more freedom in a_{ij} and b_{ijkl} . This is realized, e.g., for biaxial colloidal particles in two crossed external fields along \vec{E} and \vec{B} .

3. SIMULATION PARAMETERS

As initial condition, a square domain is defined with a sphere in the center to initialize the nucleus. Periodic boundary conditions in all directions in the square box are used.

The values for the parameters are the same as defined in [17], namely $\rho = 1$ (which sets the time scale), $a_{11} = a_{22} = 2$, $b_{1111} = b_{2222} = b_{1122} = 1$, $b_{1212} = 0$ and $c = 1$, respectively [41]. However, a typical set of values for τ and s is used for each simulation since our basic objective is to study the dependence of the stable state phase on these parameters. A simple explicit numerical scheme is used to obtain a reasonably well approximated solution. A forward Euler scheme is used for the time derivative with a sufficiently small time step of $\Delta t = 0.00075$ to ensure the stability of the scheme. The Laplace operator is approximated by using second order difference scheme given by

$$\nabla^2 \phi = (\phi_{i+1,j} + \phi_{i-1,j} + \phi_{i,j+1} + \phi_{i,j-1} - 4\phi_{i,j})/(\Delta x)^2. \quad (22)$$

For the following simulations Δx is chosen as $\Pi/4$. Convergence of our results was ensured via convergence studies. The morphologies depicted in figure 1, figure 2 and figure 4 show simulations of 256 times 256 numerical grid units. However, morphologies in figure 5 show simulation of 128 times 256 numerical grid units.

4. RESULTS AND DISCUSSION

In this section we present the simulation results obtained from our studies. These simulation results demonstrated the following issues concerning nucleation and successive microstructure formation:

- (i) The effect of undercooling on crystal growth.
- (ii) The dependence of anisotropy and undercooling on stable state phase.
- (iii) The effect of anisotropy and undercooling on distance between the neighbouring stripes.

4.1. Anisotropic effects

In order to quantify the anisotropy of the material at the atomic scale, a dimensionless parameter s is introduced and is given by

$$s = -\frac{b_{1112}}{b_{1111}}. \quad (23)$$

The effect of this dimensionless parameter is studied by performing numerical simulations with $s = 0$ and $s = 0.125$. The initial and boundary conditions as well as the values for all other simulation parameters used in these simulations as same as given in section 3. The results obtained for both cases after 30,000 time steps are shown in figure 1.

4.2. Undercooling effects

When a liquid is supercooled just below the melting temperature the crystal starts growing and the crystal growth is directly related to the undercooling. Depending on

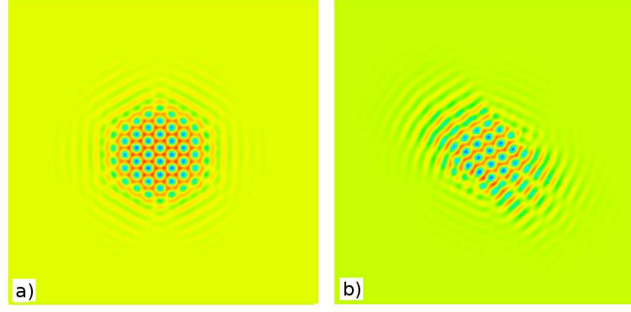


Figure 1. Simulation results of crystal growth calculated for $\tau = -3/4$ and (a) $s = 0$ (isotropic case) and (b) $s = 0.125$ (anisotropic case). All other parameters are chosen as given in section 3. As expected the isotropic case shows a symmetric morphology.

the formal undercooling, which quantifies the distance from the phase-equilibrium line in the phase diagram, in the system the final state will have different morphologies. These are categorised and analysed here in detail to get an overview of the state phase of the APFC model given by the variables s and τ .

In this section the APFC model is used to examine the rate of crystal growth from a supercooled liquid state. As explained above, τ represents the undercooling in our model. A number of simulations with different values of τ are performed for a specific s value. We used the same initial condition i.e. single solid nucleus (nucleation site) for all simulations. The results showed that the rate of crystal growth increases with an increase in the value of τ . As an example the simulation results with $s = 0$ and for two typical values of τ i.e. with $\tau = -0.25$ and $\tau = -0.8$ respectively at 40,000 time steps are depicted in figure 2.

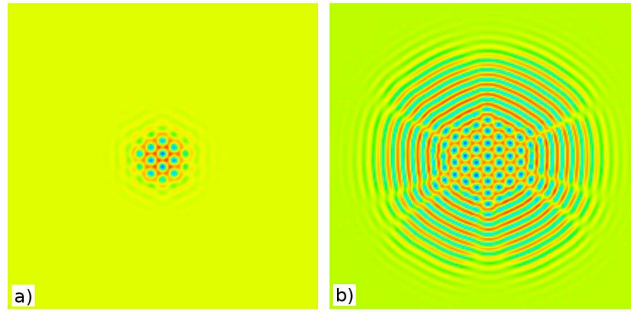


Figure 2. Simulation results of crystal growth after 40,000 time steps for $s = 0$ and (a) $\tau = -0.8$ and (b) $\tau = -0.25$

4.3. Heterogeneous nucleation and crystal growth

In this section we studied the dependence of a stable state phase on anisotropy and undercooling. More specifically, we show how a stable state can be composed of different phases such as triangular phase, stripe phase and co-existence of stripes and triangular

phase, depending on the values of s and τ i.e. anisotropy and undercooling respectively. To study these patterns we performed a number of simulations with different values of s and τ in each simulation. However, the other parameters for all these simulations are same as described in the previous section. The results in the form of a diagram of stable state phase are demonstrated in figure 3.

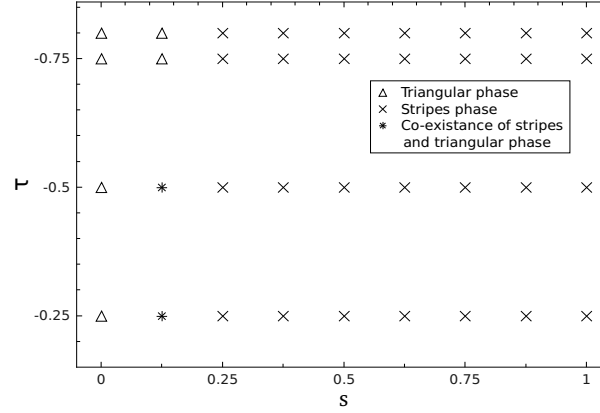


Figure 3. Simulation results of stable phases for same initial conditions and different values of s and τ

These simulation results demonstrate that the stable state phase always consists of stripes if $s \geq 0.25$ irrespective of the τ value. The co-existence of stripes and triangular phases is found only in case of $s = 0.125$ and $\tau \geq -0.5$, while for other values of s and τ , the stable state consist of a triangular phase. Typical picture of the triangular phase, stripes, and a co-existence of stripes and triangular phase are given in figure 4.

The precise shape of the grain boundary between the two solid phases depends on the system size due to [42]. The two-phase coexistence as such, however, is independent of the size of the system.

4.4. Distance between the neighbouring stripes

To analyse the stripe morphology further, we studied the effect of anisotropy and undercooling on the distance between the neighbouring stripes. As discussed in the previous section, the stable state consists of stripes when $s \geq 0.25$ irrespective of the τ value, as shown in figure 3. It is observed that the stripe phase obtained for different values of s are different from each other in terms of the spacing between the neighbouring stripes in the stripe phases. However, simulations with different values of τ result in similar stripe phases. Our results reveal that the spacing between neighbouring stripes decreases with an increase in the value of s . Thus the stripe phase obtained with $s = 1$ are much finer compared to the ones obtained with $s = 0.25$. Further, to investigate the effect of the undercooling τ on the stripe phase, we performed several simulations by fixing a specific value for s and varying τ . The results show that for a specific value of s ,

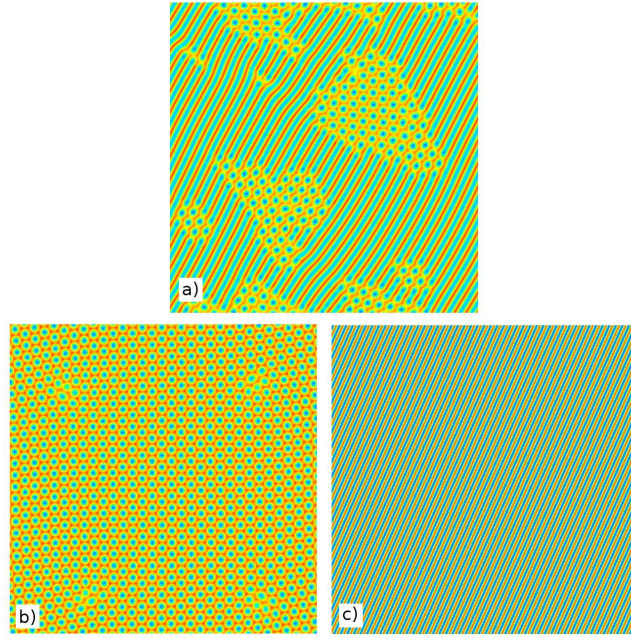


Figure 4. Typical stable states phases from simulations performed for (a) $s = 0.125$ and $\tau = -0.25$, which result in a co-existence of stripes and triangular phase, (b) $s = 0$ and $\tau = -0.75$ which result in the triangular phase, and (c) $s = 0.75$ and $\tau = -0.25$, which results in stripes

similar stripe morphologies are obtained with different value of τ . Figure 5 demonstrates this interesting finding for different values of s and τ .

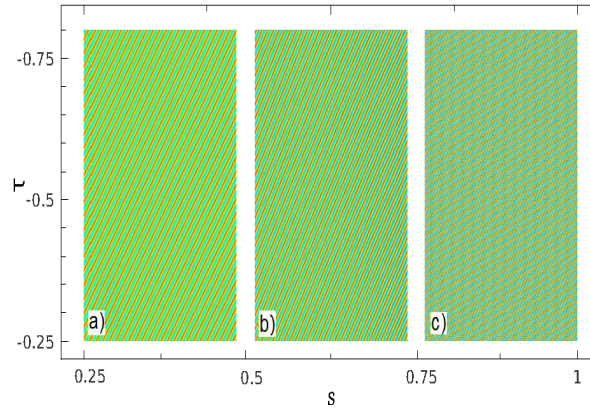


Figure 5. Stripe phases for different values of s and τ . Resulting stripe phase for (a) $s = 0.25$, (b) $s = 0.625$ and (c) $s = 1$.

From the above discussion, we can conclude that the distance between neighbouring stripes decreases as we increase the value of s . However, the undercooling has no significant effect on the stable stripe phase, i.e. the stripe phases for different values of τ are similar.

4.5. Analysis of the anisotropy introduced by s

In this section we discuss the influence of the anisotropic factor s on the final triangular phase obtained with $0 \leq s \leq 0.125$ and $\tau = -0.75$. More specifically, we analysed the form of triangles in each of the final triangular phase. The form of a triangle is determined in terms of three internal angles and ratio of length of the longest and shortest sides of the triangle. It is observed that the triangular phase obtained in case of $s = 0$ i.e. without any anisotropy, consist of triangles with same three angles of 60° each. However, the triangular phase obtained with non-zero values of s contains triangles with dissimilar sides. The details of the angles calculated for each case are shown in figure 6.

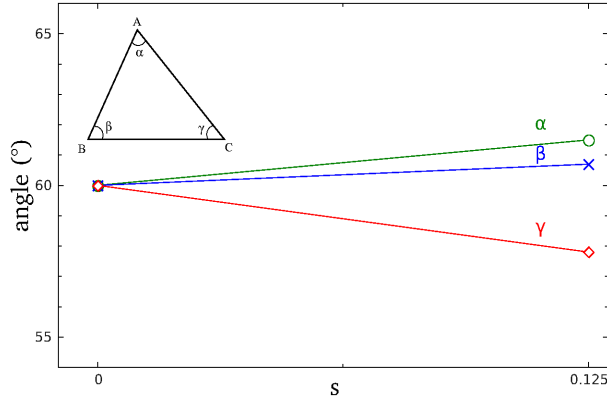


Figure 6. Form of triangles in the final triangular phase obtained for different anisotropies s .

These results demonstrate that for isotropic case i.e. $s = 0$, the final triangular phase consist of equilateral triangles. However, for anisotropic case i.e. non zero values of s , the final triangular phase contain scalene triangles i.e. no two sides are similar. The ratio of length of the longest and shortest sides of the triangles, calculated for each case is presented in figure 7. This underlines the capability of our APFC model to give rise to truly anisotropic morphologies.

5. SUMMARY AND OUTLOOK

In this article we presented a DDFT based derivation of the APFC model proposed by two of the authors (D. L. and H. E.) in [17] previously. Further we investigated the state phase of this model given by variation of τ and s to demonstrate its capacity to model structures beyond those captured by the SPFC equations originally introduced by Elder et al. [2].

In particular we studied the influence of anisotropy and undercooling on final states using numerical techniques to minimize the free energy functional in our model. More specifically, a number of numerical simulations are performed by using different sets of values for our dimensionless parameters s and τ which represent anisotropy and

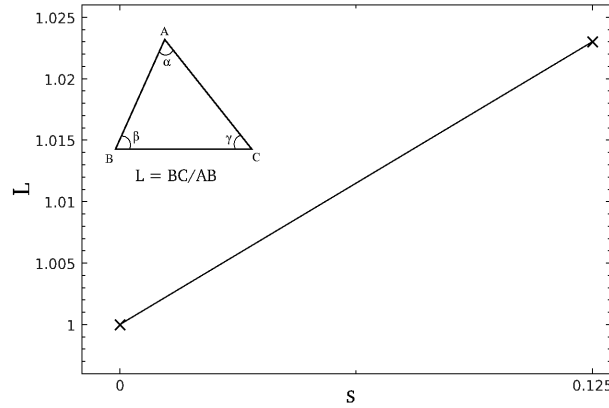


Figure 7. Ratio of the length of longest and shortest sides of the triangles in the final triangular phase versus s .

undercooling, respectively. The results obtained from these numerical simulations are analysed. Our studies reveal that:

- (i) the rate of crystal growth increases with increase of τ i.e. undercooling;
- (ii) the stable state phase consists of a stripe phase if $s \geq 0.25$ irrespective of τ . However, the stable state is a co-existence of stripes and triangular phase when $s = 0.125$ and $\tau \geq -0.5$, while for other values of s and τ , the stable state consists of a triangular phase;
- (iii) for $s \geq 0.25$, the undercooling τ has no effect on the resulting stripe phases, however, the distance between the neighbouring stripes decreases with an increase of s .
- (iv) Triangular crystals with cells that are neither equilateral nor rhombic are possible for our anisotropic model.

In the future we plan to extend the approach to reactive systems [44] to simulate morphogenesis in such systems from the atomic to microscale.

6. ACKNOWLEDGMENTS

We thank S. van Teeffelen and T. Ala-Nissila for helpful discussions. This work has been supported by the DFG through the DFG priority program SPP 1296. Daming Li is also supported by National Sciences Foundation of China (Grant No. 10701056).

References

- [1] J. Swift and P. C. Hohenberg, Phys. Rev. A **15**, 319 (1977).
- [2] K. R. Elder, M. Katakowski, M. Haataja and M. Grant, Phys. Rev. Lett. **88**, 245701 (2002).
- [3] K. R. Elder and M. Grant, Phys. Rev. E **70**, 051605 (2004).
- [4] K. R. Elder, N. Provatas, J. Berry, P. Stefanovic and M. Grant, Phys. Rev. B **75**, 064107 (2007).
- [5] P. M. Stefanovic, M. Haataja and N. Provatas, Phys. Rev. Lett. **96**, 225504 (2006).
- [6] J. Berry, M. Grant and K. R. Elder, Phys. Rev. E **73**, 031609 (2006).
- [7] K. Elder, Lecture Notes, Summer School of DFG Priority Program 1296 *Heterogenous Nucleation*, Herzogenrath, Germany, July 28th to August 1st (2008).

- [8] S. van Teeffelen, R. Backofen, A. Voigt, H. Löwen, Phys. Rev. E **79**, 051404 (2009).
- [9] H. Emmerich, Cont. Mech. Thermodyn. **15**, 197 (2003).
- [10] T. Hirouchi, T. Takaki, Y. Tomita, Comp. Mat. Science **44**, 1192 (2009).
- [11] Kuo-An Wu and A.Karma, Phys. Rev. B **76**, 184107 (2007).
- [12] A. Jaatinen, T. Ala-Nissila, J. Phys.: Condensed Matter **22**, 205402 (2010).
- [13] P. F. Tupper and M. Grant, EPL **81** 40007 (2008).
- [14] H. Löwen, J. Phys.: Condensed Matter **22**, 364105 (2010).
- [15] R. Wittkowski, H. Löwen, H. R. Brand, Phys. Rev. E **82**, 031708 (2010).
- [16] S. K. Mkhonta, D. Vernon, K. R. Elder, M. Grant, arXiv:0806.3445v2
- [17] R. Prieler, J. Hubert, D. Li, B. Verleye, R. Haberkern, H. Emmerich, J. Phys.: Condensed Matter **21**, 464110 (2009).
- [18] K. R. Elder and M. Grant, Rev. Rev. **70**, 051605 (2004).
- [19] R. Prieler, D. Li, H. Emmerich, J. Crystal Growth **312**, 1434 - 1436 (2010).
- [20] W. J. Boettinger, J. A. Warren, C. Beckermann, and A. Karma, Annu. Rev. Mater. Res. **32**, 163 (2002).
- [21] R. Evans, Adv. Physics **28**, 143 (1979).
- [22] Y. Singh, Phys. Reports **207**, 351 (1991).
- [23] H. Löwen, Physics Reports **237**, 249 (1994).
- [24] H. Löwen, J. Phys.: Condensed Matter **14** 11897 (2002).
- [25] By scaling, hard ellipsoids with fixed orientation are formally equivalent to hard-sphere systems. This is no longer true, of coarse, if the interactions are soft and involve an explicit energy scale.
- [26] A. M. Bohle, R. Holyst, T. Vilgis, Phys. Rev. Letters **76**, 1396 (1996).
- [27] H. Löwen, Phys. Rev. Letters **72**, 424 (1994); J. Chem. Phys. **100**, 6738 (1994).
- [28] T. Kirchhoff, H. Löwen, R. Klein, Phys. Rev. E **53**, 5011 (1996).
- [29] S. Prestipino, F. Saija, J. Chem. Phys. **126**, 194902 (2007).
- [30] D. van der Beek, P. Davidson, H. H. Wensink, G. J. Vroege, H. N. W. Lekkerkerker, Phys. Rev. E **77**, 031708 (2008).
- [31] V. N. Manoharan, M. T. Elsesser, D. J. Pine, Science **301**, 483 (2003).
- [32] E. Bianchi, J. Largo, P. Tartaglia, E. Zaccarelli, F. Sciortino, Phys. Rev. Letters **97** 168301 (2006).
- [33] E. Allahyarov, H. Löwen, A. A. Louis, J.-P. Hansen, Europhys. Letters **57**, 731 (2002).
- [34] E. Allahyarov, H. Löwen, J.-P. Hansen, A. A. Louis, Phys. Rev. E **67**, 051404 (2003)
- [35] M. Rex, H. H. Wensink, H. Löwen, Physical Review E **76**, 021403 (2007).
- [36] M. M. Tirado, C. L. Martinez, J. G. de la Torre, J. Chem. Phys. **81**, 2047 (1984).
- [37] H. Löwen, Phys. Rev. E **50**, 1232 (1994).
- [38] T. V. Ramakrishnan, M. Yussouff, Phys. Rev. B **19**, 2775 (1979).
- [39] K. R. Elder, N. Provatas, J. Berry, P. Stefanovic, M. Grant, Phys. Rev. B **75**, 064107 (2007).
- [40] A. Jaatinen, C. V. Achim, K. R. Elder, T. Ala-Nissila, Phys. Rev E **80**, 031602 (2009).
- [41] This choice of parameters does not correspond to a single field direction \vec{E} but to two crossed fields \vec{E} and \vec{B} , see II.C.
- [42] Note that the resulting model equations of our APFC model are not rotationally invariant – just like the ones of the famous WBK model [43]. This might cause problems when studying for example several grains and issues of their orientation with respect to each other might play an important role.
- [43] A.A. Wheeler, W.J. Boettinger, G.B. McFadden, Phys. Rev. A **45**, 7424 (1992).
- [44] B. Kutschen, K. Morawetz, S. Gemming, Phys. Rev. E **81**, 036106 (2010).